JOURNAL OF GEOPHYSICAL RESEARCH, VOL. 93, NO. A9, PAGES 9854-9866, SEPTEMBER 1, 1988

Auroral Electron Energy and Flux From Molecular Nitrogen Ultraviolet Emissions Observed by the S3-4 Satellite

M. ISHIMOTO AND C.-I. MENG

The Johns Hopkins University Applied Physics Laboratory, Laurel, Maryland

G. J. ROMICK

KIA Consultants Inc., Fairbanks, Alaska

R. E. HUFFMAN

Air Force Geophysics Laboratory, Hanscom Air Force Base, Bedford, Massachusetts

The UV spectra over the southern hemisphere nightside auroral oval have been obtained from an AFGL spectral/photometric experiment on board the low-altitude polar-orbiting S3-4 satellite. A detailed analysis of nightside auroral spectra from seven orbits between mid-May and June 1978 was performed to estimate the average energy and total energy flux of incident electrons. This study was based on observations of the N_2 LBH (3-10) (1928 Å) band and the N_2 VK (0-5) (2604 Å) band emission intensities and the application of model calculations by *Strickland et al.* [1983] and *Daniell and Strickland* [1986]. Comparison of the estimated quantities with the statistical satellite measurement of incident particles by *Hardy et al.* [1985] indicates that the LBH (3-10) band emission intensity can be used to estimate the total energy flux of incident electrons, similar to the N_2^+ 1N (0-0) (3914 Å) band emission intensity in the visible region. In addition, the ratio of the LBH (3-10) to the VK (0-5) band emission intensities indicates the average energy of incident auroral electrons in much the same way that the N_2^+ 1N (0-0) and O I (6300 Å) emission ratio does in the visible region. This study shows the use of different constituent emissions, model calculations, and synthetic spectra to infer the inherent possibilities in these types of studies.

1. INTRODUCTION

Ultraviolet (UV) auroral spectra have been studied on the basis of both rocket and satellite observations since the 1961 UV rocket spectrometer measurements (1100 and 3500 Å) [*Crosswhite et al.*, 1962] and the 1968 OGO-4 satellite observations (1200 to 3200 Å) [*Gerard and Barth*, 1976]. Investigations are mostly in the far UV (FUV) regions (< 1900 Å) with emphasis below 1400 Å. There are only a few observations in the near UV region (2000 to 3000 Å) [*Sharp*, 1971; *Beiting and Feldman*, 1979; *Huffman et al.*, 1980]. OGO-4 satellite observations [*Gerard and Barth*, 1976] revealed the auroral emissions in the N_2 Lyman-Birge-Hopfield (LBH) and N_2 Vegard-Kaplan (VK) band systems, the N I (1750 Å) line, and the O II (^4S-^2P) (2470 Å) line with 20-Å spectral resolution.

This article reports satellite measurements of nightside auroral emissions in both the discrete and the diffuse regions of the auroral oval under auroral activity conditions from quiescent to extremely active. All auroral oval observations used in this study were made over the winter southern hemisphere in darkness. The analysis concentrates on emission intensities and ratios of certain LBH and VK bands. In conjunction with model calculations [*Strickland et al.*, 1983; *Daniell and Strickland*, 1986], the UV data are used to estimate the average energy and the total energy flux of incident electrons across the auroral oval for each orbit. The results are in general agreement with the previously reported characteristics of particle precipitation across the auroral oval obtained by electron precipitation measurements [*Hardy et al.*, 1985].

The data used here were obtained by the Air Force Geophysics Laboratory Ultraviolet Backgrounds experiment, flown on the S3-4 satellite in 1978 [*Huffman et al.*, 1980]. That Air Force Space Test Program satellite was in a low-altitude polar orbit near the noon-midnight meridian plane, the nadir-viewing UV instruments observed the airglow, aurora, and solar scattered radiance of the Earth's atmosphere. The experiment consisted of two 1/4-m, *f*/5, Ebert-Fastie spectrometers (FUV from 1100 to 1900 Å and UV 1600 to 2900 Å) with synchronized scans. For each wavelength range, there were three selectable bandwidths at about 1, 5, and 30 Å. A separate photometer using interference filters recorded one of four (1216, 1340, 1550, and 1750 Å) wavelength bands. The initial results of the experiment and details of the sensors have been previously described by *Huffman et al.* [1980].

2. DATA ANALYSIS

Data from 300 orbits were in easily reviewable microfiche format and covered quiescent to extremely active magnetic periods. However, in order to analyze the data in detail, the original data tapes needed to be used. In this study, we concentrate on a few orbits selected using the following criteria. First, both spectrometers were set to the same slit width in order to examine the overlapping spectral region (1600 to 1900 Å) and also to compare instrument calibration. Second, spectrometers were set at the largest slit (corresponding to a resolution of about 30 Å) in order to detect rather weak auroral emissions. Third, a photometer was set on one of the three (1340, 1550, and 1750 Å) wavelength band interference filters to continuously monitor auroral intensity variations. Finally, seven orbits, meeting all of these criteria, were selected to cover various levels of magnetic activity (Kp = 0 to 7+).

The observations of the nightside auroral oval were made at about 270 km above the winter southern hemisphere from May 1 to June 22, 1978. Solar zenith angles, geomagnetic conditions, peak intensities of the O I 1304 Å, and $L\alpha$ emissions within the oval for these seven orbits, together with the estimated particle

Paper number 7A9017.
0148-0227/88/007A-9017$05.00

characteristics, are summarized in Table 1 and discussed more fully in section 4.

2.1. *Data Reduction*

The spectrometers have an intrinsic integration period for each wavelength step of 5 ms, and it takes 21 s to make one complete wavelength scan (i.e., 1100 to 1900 Å for the FUV and 1600 to 2900 Å for the UV). The number of data points was reduced by summing over 25 ms for the FUV spectrum and over 15 ms for the UV spectrum so that each spectral readout corresponds to the total counts in 1 Å. The 30-Å resolution spectra were insensitive to smoothing for any running mean below 20 Å. Running means of 6 and 15 Å were used to construct the FUV and UV spectra, respectively, in order to minimize the apparent counting statistical noise. After this spectral smoothing process, the counts were converted to rayleighs per angstrom (R/Å) using the calibrated instrument sensitivity and radiance scaling factors given in Figure 3 of *Huffman et al.* [1980]. The detector background noise was eliminated prior to calibration by subtracting 0.34 count per 5 ms for the FUV spectrometer measurements and 0.19 count per 5 ms for the UV spectrometer measurements so that spectral intensities in wavelength regions of no expected optical emission in the nightglow would yield a low signal level.

The spectral scan time of 21 s and the field of view of the spectrometers (11.5°) are quite large compared to the characteristic time and spatial scales of auroral display features, especially over the discrete auroral region. Consequently, it is necessary to correct each readout within a spectral scan in an attempt to compensate for any auroral intensity variations during each 21-s scan as the spacecraft moves across the auroral structure. We have tried to normalize each spectrum to a constant intensity by using data from the photometer that has a small field of view (1.65° or 0.12°) and an integration time of 10 ms. The satellite takes about 4.5 s to traverse the instantaneous viewing area of the spectrometers at the 100 km altitude of the auroral emission. Therefore the photometer data were smoothed by taking a running mean (4.5 s) to smear the photometer measurement over the 11.5° viewing angle of the spectrometers. The smoothed data, which typically vary across the scan by some 20% and at most by 150% in the diffuse auroral region, were then used to normalize the spectral intensities within each 21-s scan (hereafter called the photometer normalization).

Although the LBH and VK band emissions vary differently with incident particle energy, we assume that the intensity variation over the scan is greater than the relative spectral variation due to changes in characteristic energy. This assumption is the best approach available with this data set, and it appears to work well when the photometer monitors one of the LBH wavelength regions. However, the procedure is expected to be less effective for scans associated with rapid intensity variations such as across a sharp boundary of the auroral oval. Also, the normalization is completely meaningless for auroral emissions that do not vary proportionately to the monitored photometer band. For example, neither the geocoronal nor the auroral $L\alpha$ emission varies systematically with the LBH intensities transmitted by the 1550 and 1750 Å photometer filters since these filters transmit no $L\alpha$ emission. Less than 3% of the total intensity transmitted by (1340 Å) filter is due to $L\alpha$, the rest is primarily due to the O I (1304 Å) emission (see Figure 4 in *Huffman et al.* [1980]. Thus the observed $L\alpha$ emission intensity cannot be corrected with the photometer intensity variations within each spectral scan.

The two spectrometer ranges overlapped between 1600 and 1900 Å. However, the spectral data for wavelengths greater than 1750 Å from the FUV spectrometer were not used in this analysis because of the very low sensitivity in that wavelength region [*Huffman et al.*, 1980]. When the photometer normalization is applied to spectral data in the 1600 to 1750 Å region, where the two spectrometers overlapped, the match is quite good even though the two observations were made about 14 s apart. Furthermore, after the photometer normalization, the auroral spectral band systems that cover wide wavelength ranges (i.e., the LBH and the VK) match nominal synthetic spectra very well. Figure 1 shows the comparison of the normalized auroral spectra from the diffuse auroral region averaged over four scans (Figure 1*a*) with the synthetic VK band systems (Figure 1*b*) and with the synthetic LBH band systems (Figure 1*c*); the synthetic spectra are from *Degen* [1986]. Figure 1*a* also shows the combined spectra obtained from two separate FUV and UV spectrometers and the region of spectral overlap. In the overlap region, the spectra match very well; the deviation is less than 10%. The good agreement between the observed (Figure 1*a*) and the synthetic (Figures 1*b* and 1*c*) spectra lends credibility to the photometric normalization technique. In general, photometer normalization works well except in regions with drastic intensity changes, such as near the edges of the discrete auroral region.

Since the satellite altitude during these observations was about 260 km and we observed no anomalous LBH vibrational distributions, we disregarded vehicle glow [*Conway et al.*, 1987].

2.2. *Selection of Band Systems*

Auroral and airglow radiation consists of various molecular band systems such as the N_2 LBH, VK and Herman-Kaplan, the NO γ and δ, and the O_2 Herzberg I bands, as well as atomic lines such as the N I (1200, 1493, and 1744 Å), O I (1304 and 1356 Å), N II (2143 Å), and O II (2470 Å) lines. Two wavelength regions are particularly difficult to analyze. One is from 1500 to 1900 Å, where the relative emission intensities of the VK band system are uncertain. This will be described in detail in the next section. The other region is the O_2 Schumann-Runge continuum region from 1350 to 1750 Å where atmospheric O_2 absorbs the emissions coming from below 130 km [*Meier et al.*, 1982]. Therefore in this analysis, we have concentrated on the UV spectra above 1900 Å.

The major molecular band features in the UV spectra are the LBH and VK band systems. The rest of the auroral spectral features will be more easily distinguished by subtracting out the LBH and VK band systems from the observed spectra. The solid line in Figure 2 is the observed spectrum (Figure 1*a*) with the synthetic LBH and VK band systems subtracted. In the subtraction process, the intensities of the observed and synthetic peaks at 1928 Å for the LBH and at 2604 Å for the VK are matched. Because of uncertainties in the synthetic VK band emission intensities below 2000 Å, only the VK synthetic spectrum above 2050 Å was subtracted. There are obvious atomic features at 1744 Å (N I) and 2143 Å (N II) in Figure 2. Small features below 2050 Å (except the N I line at 1744 Å) may be part of the VK band system emission; however, they typically are smaller than those expected in the synthetic spectra by a factor of 2 or 3 (Figure 1*b*). The band features above 2500 Å are mainly from the O_2 Herzberg I band systems, which are commonly seen in the airglow outside the auroral regions. The secondary features between 1900 and 2600 Å consist of the NO δ and Herman-Kaplan band systems. The O II forbidden line at 2470 Å is not clearly distinguishable in this spectrum but is strong at other times. Its intensity can reach as

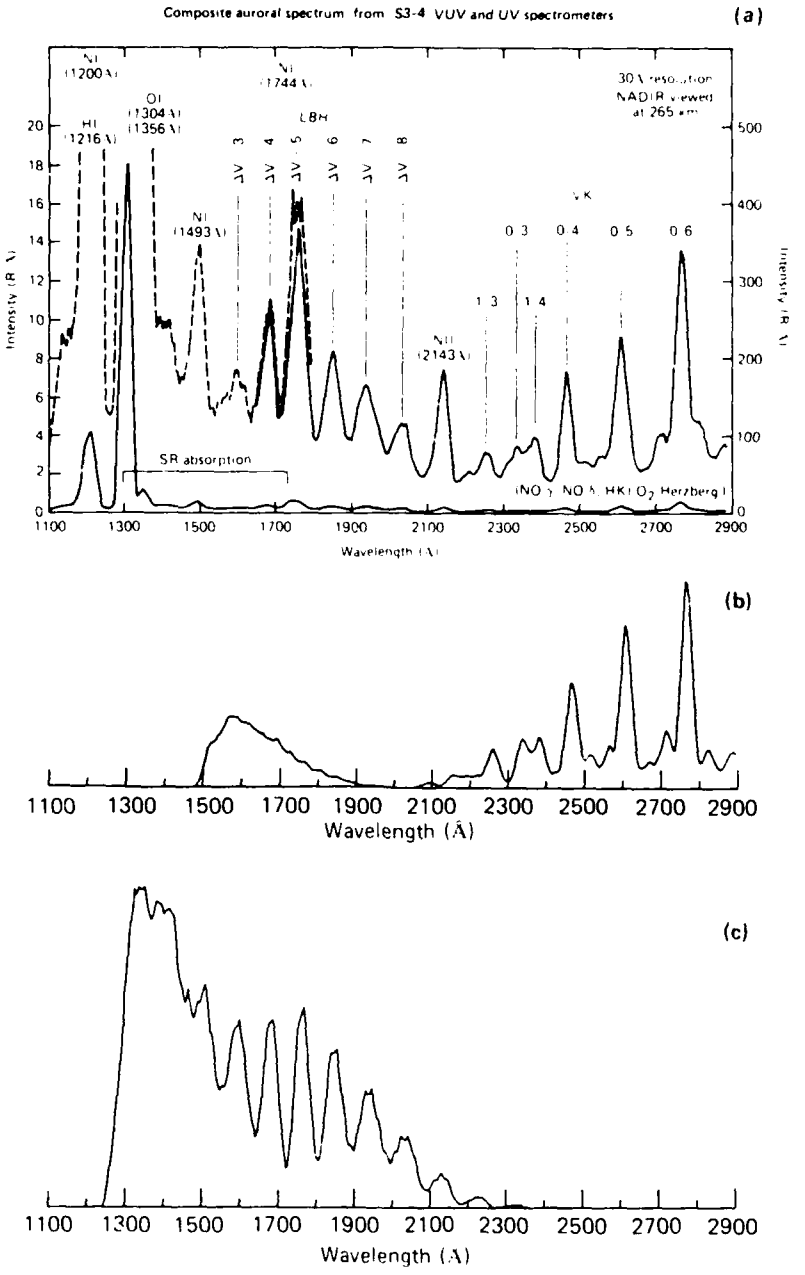

Fig. 1. Comparison of the observed UV spectrum with LBH and VK synthetic spectra from *Degen* [1986]. (*a*) Spectra of 30-Å resolution obtained by FUV (dotted line) and near-UV (solid line) spectrometers overlapping in the wavelength range 1600 to 1750 Å. These spectra are the average of four consecutive 21-s scans viewing a diffuse aurora in the southern hemisphere midnight sector from 260 km altitude at about 1836 UT on June 2, 1978. (*b*) VK synthetic spectrum assuming T_r = 400 K and the vibrational population distribution. (Note uncertainty for high v' or $\lambda < 2000$ Å; see text for details.) (*c*) LBH synthetic spectrum assuming T_r = 400 K and T_v = 400 K.

high as a few hundred rayleighs in some spectra associated with the discrete auroral region.

Taking into consideration the secondary emission band features, atomic lines, and uncertainties in the synthetic spectra, we found that the LBH (3-10) peak at 1928 Å and the VK (0-5) peak at 2604 Å are relatively free from contamination by other band systems and lines. These peaks are located outside the O_2 Schumann-Runge absorption region and have reasonably good signal strengths. Therefore these two intensities can be used as the representative emission intensities for the LBH and VK bands.

2.3. *Estimation of the LBH* (3-10) *and the VK* (0-5) *Band Intensities*

For the LBH (3-10) band intensity estimation, we integrated the observed intensity between 1916 and 1955 Å because this interval consists of LBH emission and also is the least contaminated by other emissions. The intensity of the secondary emission, i.e., NO δ, was assumed to be the same as in the nearest nightglow spectra equatorward of the oval and subtracted from this integral. For the synthetic spectra using 30-Å resolution, 99% of the LBH (3-10) band occurs in this range. In consideration of all the other

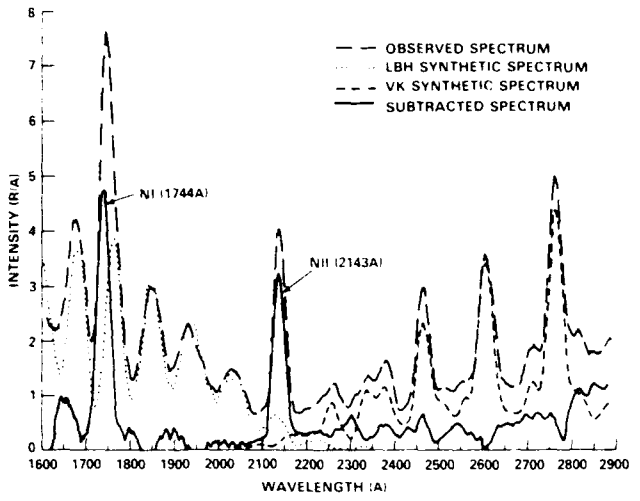

Fig. 2. The effect of subtracting LBH and VK synthetic spectra from observed UV spectra between 1600 and 2900 A. Intensities at the two peaks of 1928 and 2604 Å in the observed spectrum are used to normalize the LBH (3-10) and VK (0-5) synthetic bands. The normalized synthetic spectra are then subtracted from the observed spectrum. In the remaining spectrum, N I at 1744 Å and N II at 2143 Å are clearly seen. The spectra below 2000 Å are suspected to come from VK emission from high vibrational levels ($v' > 6$). The spectrum between 1880 and 2750 Å is a composite of the NO δ, the N_2 Herman-Kaplan band systems, and the O II forbidden line at 2470 Å. Spectra beyond 2500 Å are mainly O_2 Herzberg I band emission seen as airglow outside the auroral region.

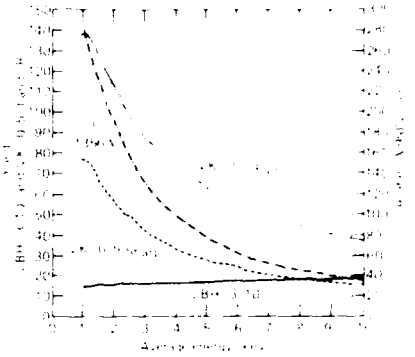

Fig. 3. The column emission rate as a function of the average energy of incident electrons calculated by Strickland: LBH (3-10), VK (0-5), and O I (1356 A). The values are normalized for a unit flux (1 erg cm^{-2} s) with a Maxwellian distribution. The MSIS-83 model atmosphere is used. The common unit for the LBH (3-10) and VK (0-5) band emission intensities is given on the left, while the unit for the O I (1356 Å) line is on the right. The subscripts of the VK (0-5)$_{\ }$ and VK (0-5)$_{\ }$ correspond to the use of the atomic quenching coefficients by *Piper et al.* [1981] and *Sharp* [1971], respectively.

overlapping LBH bands, 45.8% of the integrated intensity is due to the LBH (3-10) band. Therefore, the LBH (3-10) band emission intensity was obtained from the observed intensity integrated between 1916 and 1955 Å by multiplying by 0.463.

For the VK (0-5) band intensity estimation, we integrated the observed intensity between 2591 and 2628 Å because in this interval the VK emission is least contaminated by other emissions. The intensity of the secondary emission, i.e., Herzberg I, was assumed to be the same as in the nearest nightglow spectra equatorward of the oval and subtracted from this integral. For the synthetic spectra with 30 Å resolution, 98% of the (0-5) band occurs in this range. In consideration of all the other overlapping VK bands, 95.7% of the integrated intensity is due to the (0-5) band. Consequently, the (0-5) band emission intensit as obtained by multiplying the integrated intensity between nd 2604 Å by 0.976.

3. Model Considerations

3.1. *LBH Band System*

The LBH band system is located in the 1250 to 2400 Å range with a total intensity of 383 kR for an IBC III aurora [*Vallance-Jones*, 1974]. The LBH band system originates from a transition from the $a^1\Pi_g$ state to the $X^1\Sigma_g^+$ ground state. The collisional quenching for this band emission takes place below 95 km, which is lower than most auroral emission altitudes. A synthetic spectrum of this band provided by *Degen* [1986] is shown in Figure 1c. The model of *Strickland et al.* [1983] indicates that the peak production altitude is from 105 to 120 km, depending on the energy of the incident electrons. The LBH synthetic spectrum [*Degen*, 1986] with a 30-Å spectral resolution is not sensitive to changes in the rotational and vibrational temperature around 300 K. Consequently, we have used synthetic 30-Å spectral resolution [*Degen*, 1986] with T_r = 400 K and T_v = 400 K in this study.

Figure 3 shows the column emission intensity caused by 1 erg/cm^2 s incident flux (called yield according to Strickland) of the LBH (3-10) band as well as the VK (0-5) band and the O I (1356 Å) line as a function of the average energy of incident electrons. The energy flux with a Maxwellian distribution is more representative of the incident electron distribution in diffuse auroras as described by *Strickland et al.* [1983]. The values in Figure 3 were calculated with modified parameter values by D. J. Strickland (private communication, 1987) and differ from those in *Strickland et al.* [1983]. The cross sections of the LBH bands were replaced by those of *Ajello and Shemansky* [1985] for this calculation. The cross section of the O I (1356 Å) was adjusted by multiplying the cross section of *Stone and Zipf* [1974] by 0.6 to reflect the revision by *Zipf and Erdman* [1985]. The model atmosphere used was the MSIS-83 model by *Hedin* [1983] (year = 1985, day = 32, sec = 14,400 s, GLAT = 60°, GLON = 270°, LT = 2200, *F10.7* = 120, *AP* = 20).

Because of the direct relationship of the LBH (3-10) to the incident electrons, and because it is not dependent on chemistry, atmospheric absorption, and quenching, the yield of the LBH (3-10) band can be used with the Strickland model (Figure 3) to calculate the energy flux.

3.2. *VK Band System*

The auroral VK band system extends from 1500 to 7000 Å with a total intensity of 55 kR for an IBC III aurora according to *Vallance-Jones* [1974]. The VK band system originates in the forbidden transition from the $A^3\Sigma_u^+$ state to the $X^1\Sigma_g^+$ ground state. The VK vibrational energy levels are excited by several mechanisms such as direct electron excitation from the N_2 electronic ground state, radiative cascade involving the $B^3\Pi_g$ and $C^3\Pi_u$ states, and depopulation of the $v \geq 8$ vibrational levels by the "reverse" N_2 1P transition $A^3\Sigma_u^+ \rightarrow B^3\Pi_g$ [*Degen*, 1982]. Estimated vibrational population distributions by several studies differ from each other, especially in the high vibrational levels ($v \geq 7$) [*Cartwright*, 1978]. The dominant VK band features at wavelengths >2000 Å come from low vibrational energy levels of the N_2 $A^3\Sigma_u^+$ state that are populated largely by cascade from other electronic states. The population of the high-lying vibrational levels does not affect the band features at wavelengths >2000 Å. On the other hand, the VK band features at wavelengths <2000

Å originate from the high vibrational energy levels; however, the source and magnitude of their population distribution have not been established. If present in the aurora as it appears in the synthetic spectra, the cluster of bands in the 1500 to 2000 Å range could contribute a significant background for the LBH band systems in the same wavelength region. However, auroral spectra of 4-Å resolution obtained in a rocket experiment [*Eastes and Sharp*, 1987] show little VK band emission between 1675 and 2075 Å, where the VK emission from $v' = 4$, 6, 7, and 8 would appear. In addition, the atmospheric O_2 (Schmann-Runge continuum, 1350 to 1750 Å) absorbs the emission coming from below 130 km. Therefore considering these factors, we assumed little VK emission at wavelengths <2000 Å. The rotational energy levels appear to be collisionally well thermalized at the local temperature [*Degen*, 1982].

Because of the lifetime of the A state, it is expected that quenching will affect the emission profiles of the VK band systems. This is demonstrated in the theoretical analysis by *Daniell and Strickland* [1986]. They showed that for typical auroral average energies most of the emission will come above 120 km. According to the MSIS-83 model atmosphere [*Hedin*, 1983], the thermal temperature above 120 km during the disturbed time is greater than 400 K. The characteristic shape of VK synthetic spectra using 30-Å resolution does not vary significantly with a few-hundred-degree change in the rotational temperature above 400 K. Therefore we set $T_r = 400$ K in the synthetic spectrum by *Degen* [1986] and then used his assumed vibrational population distribution in this study (Figure 1*b*). Degen determined the vibrational population distribution by matching synthetic spectra with values from various published papers. For 30-Å resolution, the spectrum above 2000 Å in Figure 1*b* seemed adequate for this study.

Figure 3 shows the VK (0-5) band column emission intensity rates as functions of incident electron energy calculated by Strickland. The emission intensities will differ, depending on the choice of the quenching rate coefficient for atmospheric atomic oxygen for the $v' = 0$ level and the atmospheric atomic oxygen density. The quenching rate coefficients were based on rocket data, 9×10^{-11} cm^3 s^{-1} for the $v' = 0$ level by *Sharp* [1971] (hereafter called the Sharp value), and laboratory data, 2.8×10^{-11} cm^3 s^{-1} by *Piper et al.* [1981] (hereafter called the Piper value).

The variation in the atomic oxygen densities changes the column emission intensity in a way similar to the change in the quenching rate coefficient. The dependence on the atmospheric oxygen density was demonstrated in Figure 13 of *Daniell and Strickland* [1986].

In order to get atomic oxygen densities for the aurora cases studied here, the column emission intensity ratio of the O I (1356 Å) line to the LBH (3-10) band was utilized (Figure 4). Variations in the atomic oxygen densities also change the column emission intensity of the O I line as illustrated in Figure 11 of *Strickland et al.* [1983]. In the next section, we will use this concept and the observed O I (1356 Å) line emission to deduce an appropriate atomic oxygen density. The selection of the model-energy-dependent intensity relationship for the VK (0-5) band will depend upon the LBH (3-10) and the VK (0-5) bands, a suitable atomic oxygen quenching coefficient, and the atmospheric oxygen density deduced from the observed O I (1356 Å) line.

3.3. *Relation of Total Energy Flux and Average Energy of Incident Electrons, and the Observed Emission Intensities*

The average characteristics of auroral electron precipitation from data of the DMSP and STP 78-1 satellites were statistically studied as a function of magnetic local time, latitude, and the *Kp* index by *Hardy et al.* [1985]. They obtained an average energy flux of a few ergs/cm^2 s and the average energy of incident electrons was about 3 keV for $3 < Kp < 6$ in the midnight sector.

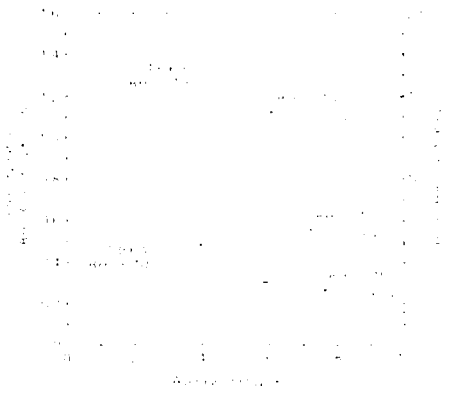

Fig. 4. Emission intensity ratios as a function of average energy of incident electrons. The ratios in solid line are deduced from the values in Figure 3. The two solid curves for the LBH (3-10) to the VK (0-5) band emission intensity ratios reflect the use of the Sharp or Piper atomic oxygen quenching coefficient. The two dotted curves demonstrate the effect of 30% atomic oxygen density of the model atmosphere (see the text for detail). The common scale of the VK (0-5) to the LBH (3-10) band emission intensity ratio is given on the left, while the scale for the O I (1356 Å) line to the LBH (3-10) band intensity ratio is given on the right. The subscripts of the VK $(0\text{-}5)_{Piper}$ and VK $(0\text{-}5)_{Sharp}$ correspond to the use of the atomic quenching coefficients by *Piper et al.* [1981] and *Sharp* [1971], respectively.

In the discrete auroral region where high total energy flux of incident electrons is expected, the S3-4 spectral data show high intensities of the LBH (3-10) band emission. Its yield is insensitive to the energy of the incident electrons (Figure 3), and thus the observed absolute emission rate is proportional to the total energy flux of incident electrons.

The LBH (3-10) band yield by an electron flux with average energy of about 3 keV is 16 R, as shown in Figure 3. The observed average LBH (3-10) band intensity for $3 < Kp < 6$ was 55 R. Thus, the average energy flux inferred from the seven orbits in the diffuse region of the southern auroral oval is 3.5 ergs/cm^2 s, which is at the higher end of the values reported by *Hardy et al.* [1985]. Considering the differences between the instantaneous and the model atmospheres, the agreement is certainly very reasonable. Thus with the Strickland model, the LBH (3-10) band intensity can provide a way of observing remotely the energy flux of auroral precipitation.

The most uncertain density in the model atmosphere is that of atomic oxygen. We can estimate the atomic oxygen density based on the observations of the O I (1356 Å) line and the LBH (3-10) and VK (0-5) band emission intensities.

In order to deduce the O I 1356-Å line intensity, the LBH bands which overlap this wavelength must be subtracted from the observed spectra. Since we do not know the altitude distribution of the LBH band emission, we cannot estimate the exact LBH band emission intensity through the O_2 SR absorption. However, we can estimate upper and lower bounds of the O I line assuming two imaginary LBH band systems.

The upper bound value of the O I intensity was estimated by subtracting our underestimated LBH band intensity around 1356 Å. Assuming the LBH emission was located in one layer at a certain altitude, we can apply the known variation of the absorption cross section as a function of wavelength [*Hudson*, 1971] to the

synthetic LBH band system spectrum and modify this synthetic spectrum to the observations between 1600 and 1680 Å. This one layer approximation always underestimates the LBH bands around the 1356 Å, where the O_2 SR cross section is large. We then subtracted this under-estimated LBH contribution from the 1356 Å observation to obtain an upper bound for pure O I (1356 Å) emission intensity.

A lower bound value for the O I intensity was estimated by subtracting our overestimated LBH band intensity around 1356 Å. In the wavelength region of 1356 Å ± 60 Å, only three nontrivial atomic lines exist, the O I 1304 Å, the O I 1356Å, and the N I 1411Å. If all the LBH band systems are subtracted from the observed spectra, these three lines should be the only ones appearing in the subtracted spectra. The two minimum intensity points between the three maximum points from the three atomic line peaks in the LBH subtracted spectrum should not be less than zero for the 30-Å resolution spectra. If we draw a straight line on the spectra between these two minimum points and assume the peak intensity of the O I line to be above this straight line at 1356 Å, we get the lower bound O I emission intensity.

Taking the middle point of the upper and lower bounds for the bottom of the O I line, we obtained the O I emission intensity. The difference between this middle point and either bound lies within 10% of the estimated O I emission intensity itself. This accuracy (within 10%) is adequate for our study. The average intensity ratio of the O I (1356Å) to the LBH (3-10) remained approximately constant at about 5 ± 1 in the diffuse auroral regions where the LBH (3-10) band intensities were more than 20 R.

Figure 4 shows the intensity ratio O I(1356Å)/LBH(3-10) as a function of the average energy of the incident electrons calculated by Strickland under a MSIS-83 model atmosphere (the values are from Figure 3). A reduction of the atmospheric oxygen density lowers the magnitude of the curve by decreasing the O I (1356 Å) line emission (see Figure 11 of *Strickland et al.* [1983] for details). The curve reads 4.5 keV for the intensity ratio of 5, observed by the S3-4 satellite. However, if the atomic oxygen density during the observations were smaller, the curve calculated for this modified oxygen density would have been reduced in magnitude, therefore the curve would have read a lower average energy for the observed intensity ratio (5).

Figure 4 also shows the intensity ratios LBH(3-10)/VK(0-5) as a function of the average energy of the incident electrons calculated by Strickland (the values are from Figure 3). These two curves in Figure 4 represent the two quenching rate coefficients with the same MSIS-83 model atmosphere. A reduction of the atmospheric oxygen density decreases the magnitude of the curve by increasing the VK (0-5) band emission, and therefore decreasing the ratio LBH/VK (see Figure 13 of *Daniell and Strickland* [1986] for details). The LBH/VK curves for Sharp and Piper quenching coefficients read 3 and 8.5 keV for the average intensity ratio of 0.4 observed by the S3-4 satellite. However, if the atomic oxygen density during the observations were smaller, the curves calculated for this oxygen density would be reduced in magnitude, and therefore yields higher average energy for the intensity ratio of 0.4.

If the atomic oxygen density during the observation was 30% less than the model atmosphere used in the Strickland calculation. (It would lower the curves O I/LBH by 30% and LBH/VK by 20% in Figure 4, according to Strickland's calculations (see Figure 11 of *Strickland et al* [1983] and Figure 13 of *Daniell and Strickland* [1986]. Then, the new curves of the O I/LBH for the intensity ratio of 5 and the LBH/VK with Sharp quenching coefficient for the intensity ratio of 0.4 would yield the same averaged energy of 3.5 keV for this reduced atomic oxygen atmosphere. Although this estimated average energy is slightly higher than the statistically averaged energy, 3 keV, reported by *Hardy et al.* [1985], we conclude that the analysis of the VK band intensity using the Sharp quenching coefficient satisfactorily links the optical measurements, the model calculations by *Strickland et al.* [1983] and *Daniell and Strickland* [1986], and the particle analysis by *Hardy et al.* [1985]. Therefore we conclude that the atomic oxygen density during our observation was 30% less than that of the MSIS-83 atmosphere used in Strickland's calculation. This shows the consistency of the observations with the results of Strickland's new LBH and VK calculations with the Sharp coefficient for the reduced atomic oxygen density.

4. Observations and Results

The seven auroral oval crossings in the midnight sector are described in this section. The observed $L\alpha$ and O I (1304 Å) emission intensities, inferred incident electron characteristics, and magnetic conditions of these orbits are presented before the description of each auroral oval pass. Table 1 lists the observation date and time, the activity indices and approximate locations of the satellite and the solar zenith angles. The emission intensities were obtained every 22 s, corresponding to the spectrometer scan cycle (the spectrometer scanning time was 21 s). Because of the small spatial (i.e., temporal) scale of emissions, the values for the discrete auroral region listed here may not necessarily be representative. However, the values for the diffuse region are representative of each orbit.

The auroral $L\alpha$ emission intensities show no correlation to the activity indices over these orbits. The geocoronal $L\alpha$ intensities show a correlation with the solar zenith angle. *Meier and Mange* [1970] reported that the geocoronal $L\alpha$ is a function of the solar zenith angle and the column hydrogen concentration at the observation point. Since the S3-4 observation altitudes were about the same for all orbits in this latitudinal region, any variation of geocoronal emission is primarily due to changes in the solar zenith angle. The O I (1304 Å) emission intensities in the diffuse region have a strong correlation with magnetic activity. The LBH and VK band emission intensities, discussed later for Figures 5*a*-5*g*, also have a correlation with magnetic activity.

The bottom part of Table 1 gives the inferred incident electron characteristics. The average energy is the incident electron energy averaged over the entire oval crossing. The highest average energy did not occur in the most disturbed period during these seven orbits. The next line, average energy flux, gives the incident energy flux averaged over the entire oval crossing. The last parameter in the table, total energy flux across the oval, gives the sum of the energy flux, each 22 s, throughout the auroral oval for each orbit in terms of ergs/cm^2 s in a 1-cm slice across the oval and also in a fan-shaped slice with 0.5 hour longitudinal width. The former value represents the emission of the exact area observed by the nadir-viewing satellite. The latter value, which is well correlated with magnetic activity, is deduced for comparison to observations of *Hardy et al.* [1985]. The total energy flux obtained for the midnight sector (2345 to 0015 MLT) varies from 3.0×10^{23} to 1.3×10^{25} keV/s sr, which is consistent with the previously reported auroral electron precipitation over these magnetic activity levels (as in Figure 8 of *Hardy et al.* [1985].

The individual orbits, described in Figures 5*a*-5*g*, illustrate the complexities in the electron energetics and proton precipitation at the various levels of magnetic activity. The figures focus on the LBH and VK bands, the auroral $L\alpha$ emission intensities, and the

TABLE 1. Summary of Geophysical Conditions

	Orbit Number						
	1216	1593	1410	1418	1401	1267	1041
Time, 1978							
month, day, hour, minute	5 30 1512	6 22 2029	6 11 0037	6 11 1401	6 11 0037	6 2 1836	5 19 2022
day, second	150 54720	173 73740	162 2220	162 50460	162 2220	153 66960	139 73320
Activity index							
Kp	2+	3+	2	1	4+	7+	0
Ap	18	15	17	10	17	82	4
*F*10.7	143	184	110	113	110	143	131
AE	300	250	200	100	350	1200	50
Dst	−34	−12	−31	−28	−35	−57	−18
Location							
Solar zenith angle	147	133	147	120	129	143	126
Altitude, km	273	264	274	273	277	295	270
Emissions, kR							
Auroral $L\alpha$							
Discrete peak	1.2	0.4	0.0	0.0	0.3	0.1	0.1
Diffuse peak	3.8	1.3	1.0	0.6	2.2	1.0	0.5
Geocoronal $L\alpha$	2.0	2.3	1.2	2.2	1.7	2.1	3.1
O I (1304 Å)							
Discrete peak	7.0	6.0	3.0	2.5	4.0	14.0	5.5
Diffuse peak	2.3	2.2	1.3	1.0	3.0	5.0	2.6
Incident electron characteristics							
Average energy, keV	3.6	4.4	1.2	3.6	5.4	3.2	3.2
Average energy flux, ergs/cm^2 s	10.0	2.2	5.2	0.66	2.5	8.6	0.78
Total energy flux across the oval 1 cm width ($\times 10^8$ ergs/s)	19.4	3.9	5.1	0.74	4.1	19.6	1.69
30 min longitudinal width ($\times 10^{23}$ keV/s sr)	122	15.2	37.1	3.38	21.9	133	3.4

photometer data. The latitudinal emission intensity variations for all seven auroral oval crossings are presented. There are four panels in each diagram. The first (top) panel shows the high-time-resolution nadir-view photometer data across the auroral oval without averaging. The value in the upper right-hand corner indicates the peak transmission wavelength of the photometer filter used for that orbit. Since each filter has a rather wide bandpass with a full width half maximum of 116 to 164 Å [*Huffman et al.*, 1980], the photometer counts of the 1340-Å filter do not necessarily covary with the LBH or VK band system intensities, owing to the strong influence of the O I (1304 Å) emission. Thus photometer normalization using this particular bandpass (1340 Å) does not work as well as when using filters centered at 1550 or 1750 Å. Also, as previously mentioned, the photometer normalization to the spectral observation is not valid in a region with sudden intensity changes (more than a factor of 10 in a few seconds), such as at the edge of the discrete auroral region.

The second panel shows the deduced auroral $L\alpha$ and N I (1200 Å) emission intensities as well as the total observed $L\alpha$ emission intensity. There are several steps in the calculation of the auroral $L\alpha$ intensity from the observed spectrum. We first deduced the N I (1744 Å) emission intensity by subtracting Degen's synthetic spectrum from the observed LBH band intensities between 1715 and 1775 Å. Second, the ratio 4.0 of the cross sections of N I lines at 1200 and 1744 Å was used to estimate the N I (1200 Å) line intensity. This ratio from the laboratory [*Ajello and Shemansky*, 1985] and from atmospheric observations [*Gerard and Barth*, 1976; *Sharp and Rees*, 1972] varies from 4 to 7. The differences are primarily due to the optical thickness of the N I (1200 Å) [*Meier et al.*, 1980] and the height of the aurora. The N I (1200 Å) emission intensity deduced in this way also has to be corrected for possible changes within the spectral scan as described previously. Third, we integrated the intensities of the spectra over the wavelength interval 1200 to 1245 Å without photometer normalization (hereafter called integrated 1216 Å), and we subtracted the corrected deduced N I (1200 Å) from the integrated 1216 Å. Assuming that the geocoronal $L\alpha$ change is very smooth and that its intensity can be linearly interpolated across the auroral region, it is subtracted from the integrated 1216 Å in order to obtain the auroral $L\alpha$ intensity within each spectral scan. However, this process introduces some uncertainties into the determination of the N I (1200 Å) emission intensity because of the photometer normalization and the fixed ratio that we used for the N I line emissions at 1200 and 1744 Å. Because of the potential large error due to large intensity change across the spectrum, both $L\alpha$ and N I (1200 Å) emission intensities in the discrete auroral region were not plotted in Figures 5*a*-5*g*. In general, the deduced auroral $L\alpha$ variation across the auroral oval is as expected: a general increase toward the equatorward edge of the diffuse region and a general but not well defined overall enhancement with increasing activity.

The third panel shows the emission intensities of the LBH (3-10)

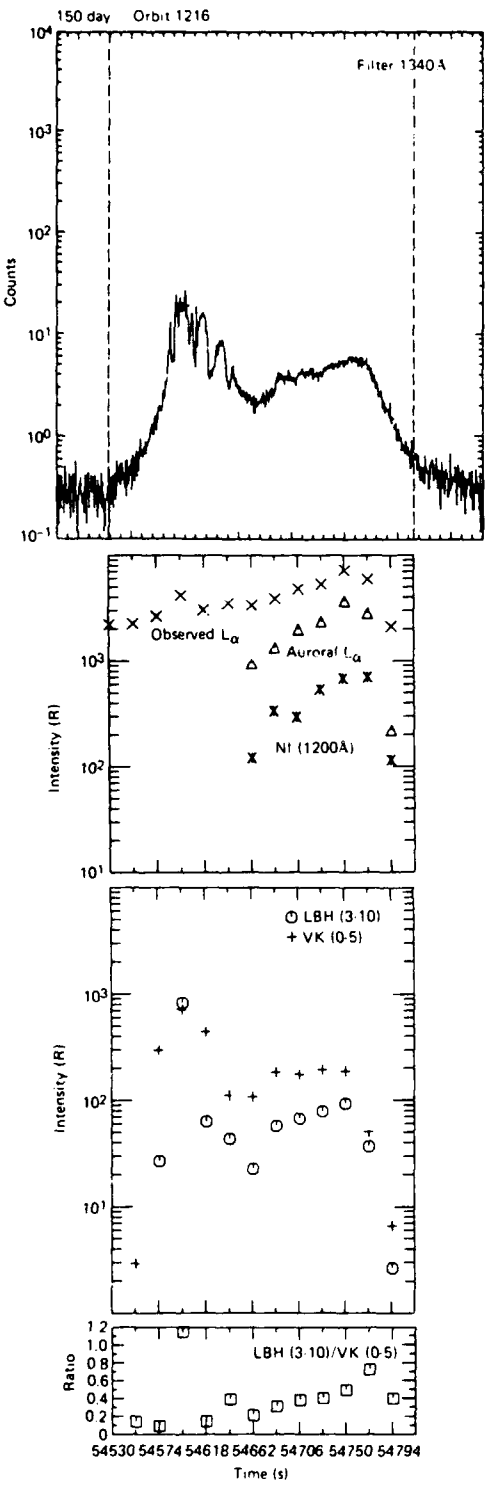

ALT (km)	277.4	276.7	275.7	274.5	273.2	271.6
GCLAT	-64.0	-60.8	-57.5	-54.3	-51.0	-47.7
GCLONG (+E)	122.5	120.5	118.9	117.5	116.3	115.2
CMLAT	-75.3	-72.2	-69.0	-65.8	62.6	-59.4
GMLONG (+E)	200.1	195.2	191.9	189.3	187.3	185.6

Fig. 5a

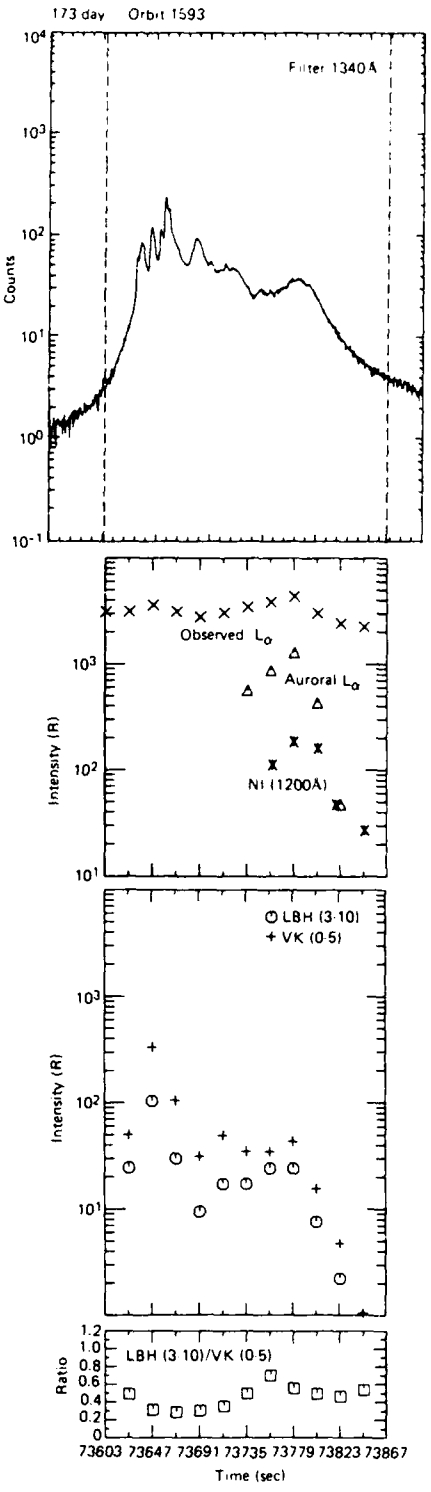

ALT (km)	269.8	270.0	270.0	269.7	269.2	268.3	267.3
GCLAT	-80.7	-78.1	-75.2	-72.2	-69.0	-65.8	-62.6
GCLONG (+E)	74.6	62.5	54.8	49.6	45.9	43.2	41.0
GMLAT	-82.8	-80.3	-77.4	-74.2	-71.0	-67.8	-64.5
GMLONG (+E)	50.5	66.0	74.6	79.7	83.0	85.1	86.7

Fig. 5b

Fig. 5. Latitudinal (time) variation of LBH (3-10) and VK (0-5) emission intensities for the seven orbits. Top panel, observed photometer counts. Second panel, both the total observed $L\alpha$ emission (cross) and the auroral $L\alpha$ emission (triangle), and the N I (1200 Å) emission (star). Third panel, LBH (3-10) (circle) and VK (0-5) (plus) band emission intensities. Fourth panel, intensity ratio of LBH (3-10) to VK (0-5) band emission intensities.

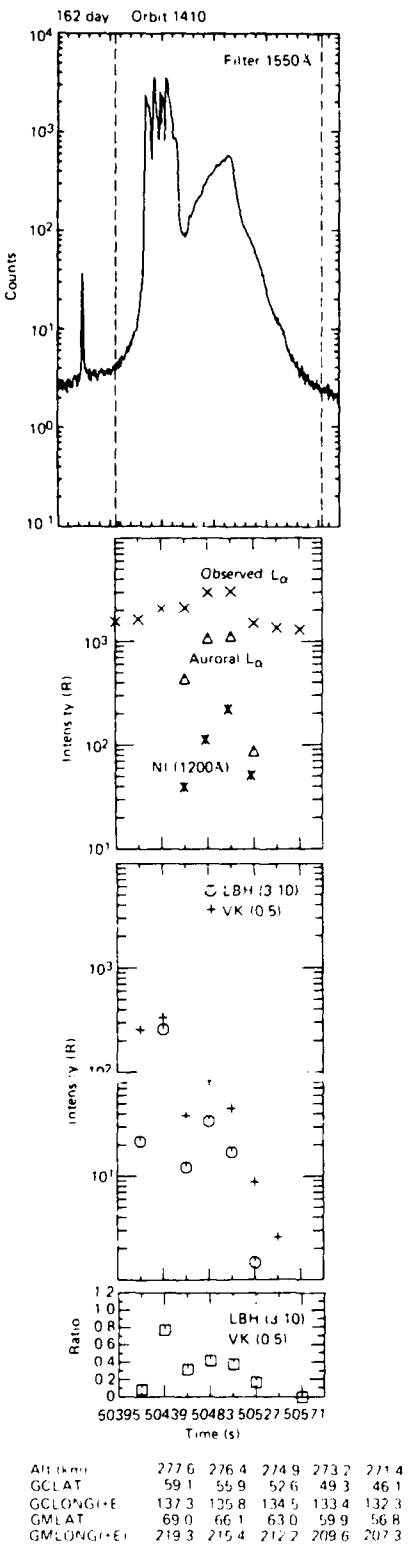

Fig. 5c

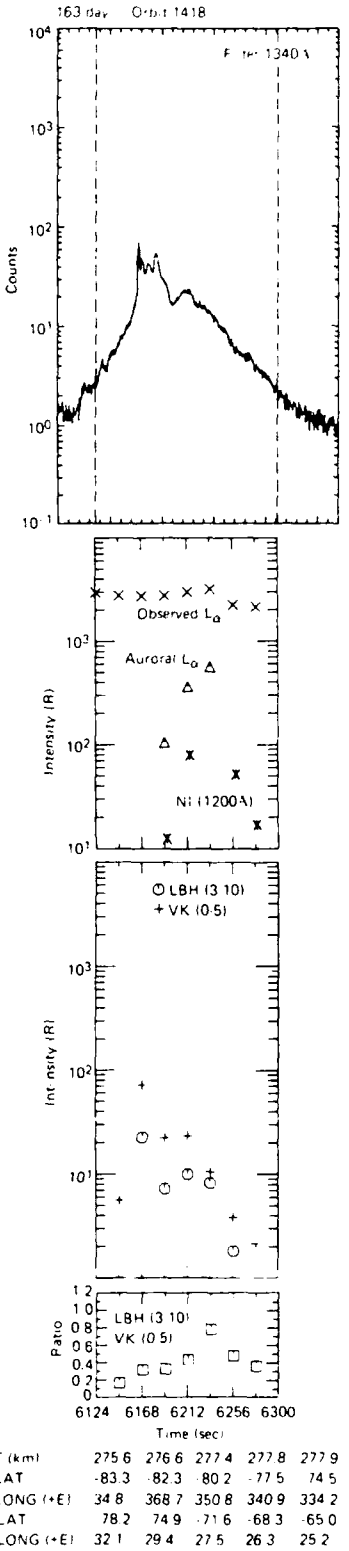

Fig. 5d

and VK (0-5) bands. In the process of deducing these intensities, the NO δ band and the O_2 Herzberg I band emission intensities were subtracted from the 1916 to 1955 Å integral for the LBH (3-10) emission intensity and from the 2591 to 2628 Å integral for the VK (0-5) emission intensity, respectively. The background emission of the NO δ (1 to 2 R) and the O_2 Herzberg I band (3 to 9 R) within the auroral oval was determined from the airglow intensity measured just outside the equatorward edge of each auroral region. These observed intensities are only a few rayleighs for the LBH (3-10) band region and less than 10 R for the VK

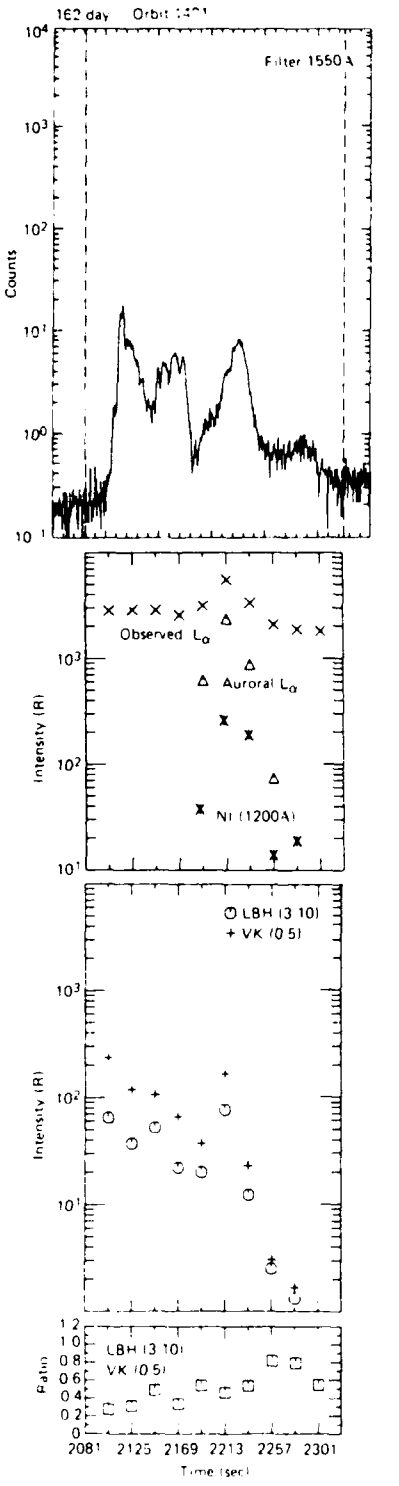

ALT (km)	281.3	281.0	282.4	282.6	282.5	282.1
GCLAT	80.8	78.2	75.3	72.2	69.1	65.9
GCLONG (+E)	371.5	360.3	352.9	347.8	344.0	341.2
GMLAT	74.2	70.9	67.6	64.2	60.9	57.6
GMLONG (+E)	35.0	35.3	35.5	35.5	35.5	35.5

Fig. 5e

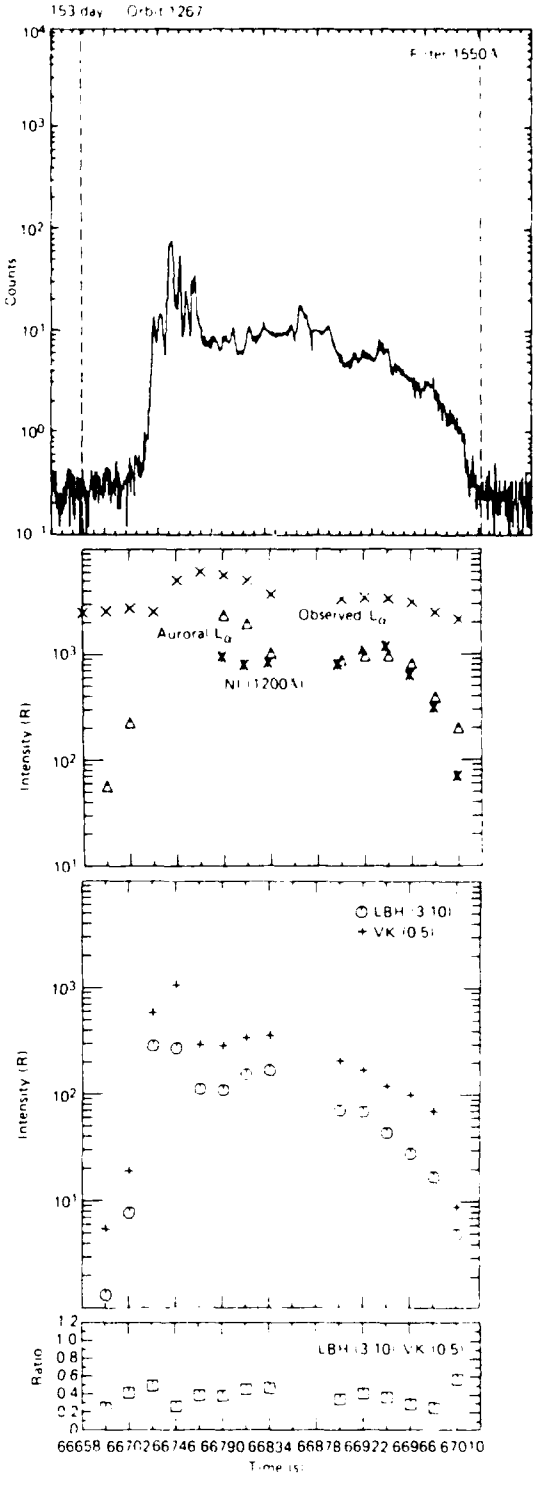

ALT (km)	281.3	281.0	280.5	279.7	278.7	277.5	276.0	274.4
GCLAT	68.4	65.2	62.0	58.8	55.5	52.2	49.0	45.7
GCLONG (+E)	75.2	72.5	70.3	68.7	67.2	65.9	64.8	63.8
GMLAT	76.2	72.9	69.6	66.2	62.9	59.6	56.2	52.9
GMLONG (+E)	115.8	117.9	119.3	120.2	120.9	121.4	121.8	122.0

Fig. 5f

(0-5) band region and were subtracted from the auroral spectra. The LBH and VK data in the third panel have been normalized within each spectral scan on the basis of the photometer data.

The fourth panel shows the intensity ratio of the LBH (3-10) to VK (0-5) band emissions from the third panel. In general, the ratio increases equatorward in the diffuse region, indicating hardening of the electron energy.

Figure 5*a* (orbit 1216) illustrates an oval crossing almost exactly along the 2300 MLT meridian plane in a period of weak activity ($Kp = 2+$) and near the peak of a small 250 nT substorm.

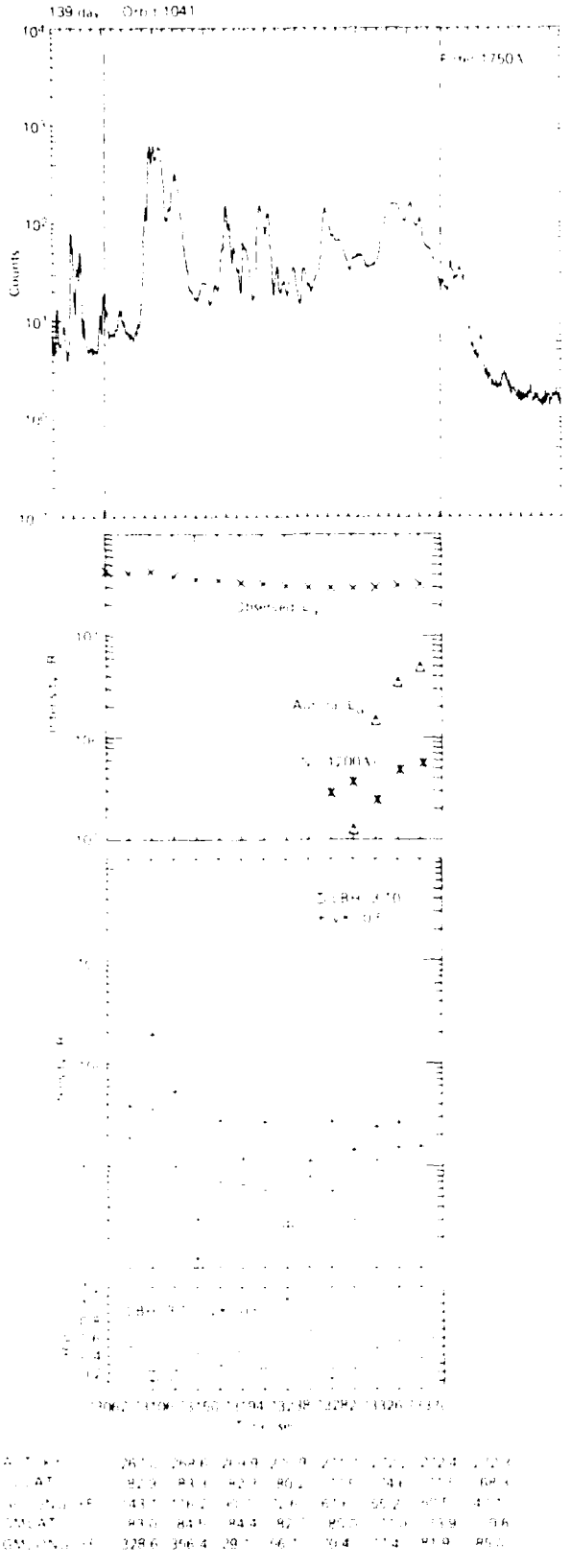

Fig. 5a

The first panel shows the auroral oval extended from ~75° to 60° geomagnetic latitude (GMLAT); a clear distinction between the discrete and diffuse auroral regions can be seen in the 1340-Å photometer intensity features.

The auroral $L\alpha$ emission intensity (second panel) in this pass is the highest among the seven orbits examined. Missing values for the auroral $L\alpha$ emission intensities are due to overestimation of the N I (1200 Å) emission intensity. The auroral N I (1200 Å) emission was subtracted as previously described. The assumed fixed ratio between the 1200 and 1744 Å emission can cause an overestimate of N I (1200 Å) at times. In the discrete region, the assumed 1200/1743 Å ratio can lead to an uncertainty in the auroral $L\alpha$ emission intensity of ±50%; however, in the diffuse region it results in only a ±10% uncertainty.

The enhancement of the auroral $L\alpha$ emission (in particular, the intensity of 3.3 kR at 54,750 s in the diffuse region) indicates proton precipitation with an energy flux of 0.4 erg cm^{-2} s^{-1}, assuming typical average energies near 10 keV (*Edgar et al.* [1973] and the $L\alpha$ cross section from *Van Zyl and Newman* [1988]. This proton flux would produce about 7 R of the LBH (3–10) and less than 1 R of the VK (5–10) band emission intensity using the curve of Figure 7 and Table 3 by *Edgar et al.* [1973] and the $L\alpha$ cross section obtained by *Van Zyl and Newman* [1988].

The third panel shows the LBH (3–10) and VK (0–5) band emission intensities with variations similar to those of the photometer. Since the photometer filter was set at 1340 Å, the reliability of the values of the LBH and VK band emission intensities in the discrete region in the third and fourth panels is lessened, even though high intensities are present in the discrete region, with input energy fluxes exceeding 60 ergs cm^{-2} s^{-1}. The energy flux in the diffuse region is 2 to 8 ergs cm^{-2} s^{-1}. Despite a rather small Kp value (2+), the total energy flux across the oval is as large as that of the intense storm (Kp = 7+) recorded among the seven cases under study here. The fourth panel shows the LBH to VK band emission intensity ratio, which is an indicator of the average energy of incident electrons. Although the value in the discrete region is less reliable owing to sudden changes in auroral intensity and a less reliable 1340-Å photometer normalization, a high average energy was still inferred. The hardening of the electron energy spectrum from 1 to 7 keV is observed across the diffuse region toward lower latitude.

Figure 5*b* (orbit 1593) shows a slanted oval crossing between the 2000 and 2130 MLT meridians in a moderately active period (Kp = 3+, AE = 250 nT) during the recovery of a 700 nT substorm. The auroral oval was located between −80° and −70° GMLAT. Although the 1340-Å photometer did not show a distinct transition between the discrete and diffuse region, the LBH and VK emission intensity variations reveal a clear transition. The auroral $L\alpha$ emission intensity profile indicates intense proton precipitation in the equatorward part of the diffuse region. The peak energy flux (third panel) and the peak average energy (fourth panel) of incident electrons are located at a slightly higher latitude than the peak in $L\alpha$. The inferred energy flux is low despite a rather active period (Kp = 3+), possibly due to the observation in the early evening sector. In the fourth panel, the inferred average energy of the incident electrons does not show very high energies in the discrete region. Hard electron precipitation in the diffuse region is evident. The last data points at 73,823 and 73,855 s in the third and the fourth panels may be in considerable error owing to the low count rate.

Figure 5*c* (orbit 1410) shows an oval crossing between the 0100 and 2300 MLT meridians in a rather low activity period (Kp = 2) during the development of a weak (<200 nT) substorm. The auroral emission was bounded between −67° and −60° GMLAT. The photometer's 1550-Å filter used on this pass basically monitored the LBH band emission. The photometer count variation

is similar to the spectrometer LBH band emission intensities. The photometer normalization in this case should work reasonably well. Auroral $L\alpha$ emission intensities peak again slightly equatorward of the LBH and VK emission intensities. At 50,439 s, the satellite was over the discrete region for almost 22 s, corresponding to one spectrometer scan cycle; therefore, the spectrum taken there represents the discrete auroral emission. Missing values of the auroral $L\alpha$ emission intensity on the second panel are due to overestimation of the N I (1200 Å) emission intensity for geocoronal background subtraction. The observed N I (1744 Å) at that time was over 1 kR. Since the 1750-Å region in the UV and the 1200 Å region in the FUV were monitored at about the same time by the two spectrometers (the photometer correction between them was only a factor of 1.1), the photometer normalization should not really affect the determination of these two emission intensity ratios. The oversubtraction of the N I (1200 Å) suggests that the intensity ratio of 4.0 is an overestimate for this discrete aurora at 50,439 s. Over this spectral scan, the photometer normalization factor changed smoothly by a factor of 3.5 compared to 3 orders of magnitude in some other discrete regions. Therefore the determined intensities of the LBH (3-10) and VK (0-5) band emissions should be fairly accurate for this discrete auroral observation. An apparent inverted V structure in electron precipitation in the discrete auroral region can be seen on both the third and fourth panels. Even though the diffuse region was very narrow, the energy hardening is still identifiable, and the average energy of 3 keV agrees well with the value from the statistical study of electron precipitation by *Hardy et al.* [1985].

Figure 5*d* (orbit 1418) shows an oval crossing near the 2300 MLT meridian in a very quiet period (Kp = 1-, AE = 50 nT) with no substorm activity in the previous 12 hours. The auroral oval was bounded between −83° and −80° GMLAT. The spectrometer recorded the weakest O I 1304 Å and $L\alpha$ line emission among the seven auroral oval crossings examined. The missing points of the auroral $L\alpha$ and LBH band emissions at 6146 and 6278 s are located below the 10 R minimum value of the figure. The inferred electron energy flux was peaked more poleward than the auroral $L\alpha$ emission and the average energy of incident electrons; however, the ratio at 6234 s may be inaccurate because of the low LBH and VK band intensities. The observed intensities of the LBH and VK band emissions were very small over the whole pass compared to other passes. Even so, energy hardening of electron precipitation in the diffuse auroral region is still recognizable.

Figure 5*e* (orbit 1401) shows an oval crossing along the 2300 MLT meridian in an active period (Kp = 4+, AE = 400 nT) during a period of continuous substorm activity. The oval was 9° wide bounded between −79° and −70° GMLAT. The photometer data do not show a clear distinction between the discrete and the diffuse auroral regions. The 1550-Å photometer observation provides reasonably good normalization for the LBH and VK band emission intensities except at 2103 s, where the emission intensities rose suddenly at the polar edge of the discrete aurora. Despite the active period, the signals were weak and the inferred energy fluxes were less than those in orbit 1410 at weak geomagnetic activity. The signals after 2257 s may not be reliable owing to a very low count rate. Nevertheless, the hardening of electron energy in the diffuse region is again obvious.

Figure 5*f* (orbit 1267) shows an oval crossing between the 2000 and 2200 MLT meridians in an extremely active period (Kp = 7+) near a peak of a very intense substorm activity. The AE index indicates that the observation was made after substorm breakup and 5 hours into intense continuous substorms. The AE value reached 1200 nT, and the oval was bounded between −73° and −53° GMLAT with a peak intensity of O I (1304 Å) of 14 kR in the discrete auroral region and 5 kR in the diffuse auroral region (Table 1). The inferred total energy flux was the largest among the seven auroral oval crossings examined. The 1550-Å photometer measurements do not show a clear distinction between the discrete and the diffuse regions; a narrow discrete region may be inferred. Two spectrometer data points at 66,856 and 66,878 s are missing in the original record. The proton precipitation was not significantly enhanced despite the active period. If we compare this with the intensity profiles of the LBH and VK band emissions, we can conclude that relatively more auroral $L\alpha$ emission was detected at the equatorward part of the oval. There is an intensity peak of the $L\alpha$ emission at the equatorward edge of the diffuse region at 66,966 s. The inferred electron energy flux in the oval crossing is between 2 and 20 ergs/cm^2 s. The hardening of electron energy is not seen, and a relatively constant average level is observed over the whole oval.

Figure 5*g* (orbit 1041) shows a slanted crossing between the 1700 and 2100 MLT meridians in a quiescent period (Kp = 0, AE < 20 nT) with no indication of substorm activity. The oval was located above about −69° GMLAT with a width of at least ~15°. The spectrometer count rate associated with this quiescent period is very low. Consequently, half of the data points for the auroral $L\alpha$ line and the LBH and VK band emission intensities are not very accurate. The average energy flux as well as the total energy flux over the whole oval are very low, as shown in Table 1. The energy flux is slightly higher in the discrete region near 2 erg/cm^2 s at 73,106 s. Even with the low signals, the proton precipitation is enhanced near the equatorward edge, and the electron energy also hardens near the edge of the diffuse region.

In summary, these seven orbits indicate that the O I (1304 Å) line emission intensity and the inferred characteristics of incident electrons are correlated with geomagnetic activity. The geocoronal $L\alpha$ line emission intensity variations are a function of solar zenith angle. The auroral $L\alpha$ line emission intensity, which is an indicator of proton precipitation, does not correlate well with the geomagnetic activity. Morphologically, the auroral $L\alpha$ emission is more intense near the equatorward edge of the diffuse region. The intensities of the LBH (3-10) and VK (0-5) band emissions are not always correlated with the geomagnetic activity. The average energy flux, total energy flux, and average energy across each oval crossing inferred from the emissions (in Table 1) are consistent with those from a statistical study of electron precipitation [*Hardy et al.*, 1985]. The increase in average electron energy was seen near the equatorward edge of the diffuse regions in most of the oval crossings.

5. Conclusions and Comments

The nadir-viewing UV spectral photometric measurement from the S3-4 satellite at 270 km provides data to study the energetics of incident electrons in the nighttime aurora. The observations of seven selected auroral oval crossings and model calculations revealed several salient features.

1. The observed emission intensities of the LBH (3-10) band, the VK (0-5) band, and the O I (1356 Å) line in the diffuse auroras were consistent with what would be inferred from a modified version of the model calculation by *Strickland et al.* [1983], provided (1) The average energy of incident electrons was 3 ± 1 keV as reported by *Hardy et al.* [1985] in his statistical study, (2) The atmospheric atomic oxygen density was 30% less than the model atmosphere (MSIS-83) used in the model calculation by Strick-

land, and (3) The atomic oxygen quenching coefficient for the VK (0-5) band by *Sharp* [1971] is used.

2. The LBH (3-10) band emission intensity is a good indicator of the average energy flux of the incident electrons. The modified model calculation produces 16 R of the LBH (3-10) band emission per erg/cm^2 s of incident electrons.

3. The intensity ratio of the LBH (3-10) to VK (0-5) emissions is a good indicator of the average energy of the incident electrons in the auroral region.

4. In the midnight sector the auroral $L\alpha$ emission is most intense near the equatorward edge of the diffuse auroral region, which is in agreement with the accepted morphology of proton precipitation and observations of ground-based Balmer emissions.

An application of the observed characteristics in the apparent near independency of the LBH band emission intensities outside the O_2 Schumann-Runge continuum on the incident electron energy (> 1 keV at least) is that auroral oval images in such LBH bands (such as the (3-10)) could be used to deduce the total energy flux precipitated within the oval. With less uncertainty and simultaneous observation of the accurate atomic oxygen densities and further understanding of the quenching rate coefficient, the simultaneous auroral oval images of LBH and VK band emissions could provide average energy contours of the oval precipitation.

The S3-4 data hold promise for future studies of the relation between proton precipitation and associated emissions. In addition, higher-resolution data (5-Å resolution) should permit a more detailed study of the relative intensities of the various N I, N II, and O II lines and $L\alpha$ emissions as well as provide detailed information on the population distributions of the VK for the high-lying vibrational levels.

Acknowledgments. We are grateful to D. J. Strickland for running his program of electron aurora for us. This research is supported by Directorate of Chemical and Atmospheric Sciences grant AFOSR 86-0057 to The Johns Hopkins University Applied Physics Laboratory.

The Editor thanks I. C. McDade and another referee for their assistance in evaluating this paper.

REFERENCES

Ajello, J. M., and D. E. Shemansky, A reexamination of important N_2 cross sections by electron impact with application to the dayglow: The Lyman-Birge-Hopfield band system and N I (119.99 nm), *J. Geophys. Res.* 90(A10), 9845-9861, 1985.

Beiting, E. J., and P. D. Feldman, Ultraviolet spectrum of the aurora (2000-2800 Å), *J. Geophys. Res.*, *84*, 1287-1296, 1979.

Cartwright, D. C., Vibrational populations of the excited states of N_2 under auroral conditions, *J. Geophys. Res.*, *83*(A2), 517-531, 1978.

Conway, R. R., R. R. Meier, D. F. Strobel, and R. E. Huffman, The far ultraviolet vehicle glow of the S3-4 satellite, *Geophys. Res. Lett.*, *14*, 628-631, 1987.

Crosswhite, H. M., E. C. Zipf, Jr., and W. G. Fastie, Far-ultraviolet auroral spectra, *J. Opt. Soc. Am.*, *6*, 643, 1962.

[illegible]ell, R. [illegible]., Jr., and D. J. Strickland, Dependence of auroral middle UV emissions on the incident electron spectrum and neutral atmosphere, *Geophys. Res.*, *91*(A1), 321-327, 1986.

Degen, V., Synthetic spectra for auroral studies: The N_2 Vegard-Kaplan band system, *J. Geophys. Res.*, *87*(A12), 10,541-10,547, 1982.

Degen, V., Dialup facility for generating auroral and airglow synthetic spectra, Rep. UAG-R(305), Geophys. Inst., Fairbanks, Alaska, April 1986.

Eastes, R. W., and W. E. Sharp, Rocket-borne spectroscopic measurements in the ultraviolet aurora: The Lyman-Birge-Hopfield bands, *J. Geophys. Res.*, 92(A9), 10,095-10,100, 1987.

Edgar, B. C., W. T. Miles, and A. E. S. Green, Energy deposition of protons in molecular nitrogen and applications to proton auroral phenomena, *J. Geophys. Res.*, *78*(28), 6595-6606, 1973.

Gerard, J.-C., and C. A. Barth, OGO-4 observations of the ultraviolet auroral spectrum, *Planet. Space Sci.*, *24*, 1059-1063, 1976.

Hardy, D. A., M. S. Gussenhoven, and E. Holdman, A statistical model of auroral electron precipitation, *J. Geophys. Res.*, *90*(A5), 4229-4248, 1985.

Hedin, A. E., A revised thermospheric model based on mass spectrometer and incoherent scatter data: MSIS-83, *J. Geophys. Res.*, *88*(A12), 10,170-10,188, 1983.

Hudson, R. D., Critical review of ultraviolet photoabsorption cross sections for molecules of astrophysical and aeronomic interest, *Rev. Geophys.*, *9*(2), 305-406, 1971.

Huffman, R. E., F. J. LeBlanc, J. C. Tarrabee, and D. E. Paulsen, Satellite vacuum ultraviolet airglow and auroral observations, *J. Geophys. Res.*, *85*(A5), 2201-2215, 1980.

Meier, R. R., and P. Mange, Geocoronal hydrogen: An analysis of the Lyman-Alpha airglow observed from OGO-4, *Planet. Space Sci.*, *18*, 803-821, 1970.

Meier, R. R., D. J. Strickland, P. F. Feldman, and E. P. Gentieu, The ultraviolet dayglow, 1, Far UV emission of N and N_2, *J. Geophys. Res.*, *85*(A5), 2177-2184, 1980.

Meier, R. R., R. R. Conway, P. D. Feldman, D. J. Strickland, and E. P. Gentieu, Analysis of nitrogen and oxygen far ultraviolet auroral emissions, *J. Geophys. Res.*, *87*(A4), 2444-2452, 1982.

Piper, L. G., G. E. Caledonia, and J. P. Kennealy, Rate constants for deactivation of $N_2(A\ ^3\Sigma_u^+,\ v' = 0,1)$ by O, *J. Chem. Phys.*, *75*, 2847-2852, 1981.

Sharp, W. E., Rocket-borne spectroscopic measurements in the ultraviolet aurora: Nitrogen Vegard-Kaplan bands, *J. Geophys. Res.*, *76*, 987-1005, 1971.

Sharp, W. E., and M. H. Rees, The auroral spectrum between 1200 and 4000 Å, *J. Geophys. Res.*, *77*, 1810, 1972.

Stone, E. J., and E. C. Zipf, Electron impact excitation of the ^3S and ^5S states of atomic oxygen, *J. Chem. Phys.*, *60*, 4237, 1974.

Strickland, D. J., J. R. Jasperse, and J. A. Whalen, Dependence of auroral FUV emissions on the incident electron spectrum and neutral atmosphere, *J. Geophys. Res.*, *88*(A10), 8051-8062, 1983.

Vallance-Jones, A., *Aurora*, D. Reidel, Hingham, Mass., 1974.

Van Zyl, B., and H. Neumann, Lyman-α emission cross sections for low-energy H and H^+ collisions with N_2 and O_2, *J. Geophys. Res.*, *93*, 1023-1027, 1988.

Zipf, E. C., and P. W. Erdman, Electron-impact excitation of atomic oxygen: Revised cross section values, *Eos Trans. AGU*, *66*(18), 321, 1985.

R. E. Huffman, Air Force Geophysics Laboratory, Hanscom Air Force Base, Bedford, MA 01731.

M. Ishimoto and C.-I. Meng, The Johns Hopkins University Applied Physics Laboratory, Johns Hopkins Road, Laurel, MD 20707.

G. J. Romick, KIA Consultants Inc., Fairbanks, AK 99775.

(Received March 19, 1987;
revised March 3, 1988,
accepted March 23, 1988.)

UNCLASSIFIED

SECURITY CLASSIFICATION OF THIS PAGE

REPORT DOCUMENTATION PAGE

1a. REPORT SECURITY CLASSIFICATION UNCLASSIFIED	1b. RESTRICTIVE MARKINGS N/A
2a. SECURITY CLASSIFICATION AUTHORITY N/a	3. DISTRIBUTION/AVAILABILITY OF REPORT APPROVED FOR PUBLIC RELEASE; DISTRIBUTION UNLIMITED
2b. DECLASSIFICATION/DOWNGRADING SCHEDULE N/A	
4. PERFORMING ORGANIZATION REPORT NUMBER(S) NONE	5. MONITORING ORGANIZATION REPORT NUMBER(S) GL-TR-89-0237
6a. NAME OF PERFORMING ORGANIZATION JOHNS HOPKINS UNIVERSITY/ APPLIED PHYSICS LAB.	6b. OFFICE SYMBOL (If applicable) N/A
6c. ADDRESS (City, State, and ZIP Code) Laurel, Maryland	7a. NAME OF MONITORING ORGANIZATION Geophysics Laboratory
	7b. ADDRESS (City, State, and ZIP Code) Hanscom AFB Massachusetts 01731-5000
8a. NAME OF FUNDING/SPONSORING ORGANIZATION GL	8b. OFFICE SYMBOL (If applicable) LIU
8c. ADDRESS (City, State, and ZIP Code)	9. PROCUREMENT INSTRUMENT IDENTIFICATION NUMBER MIPR FY7121-89-00023
	10. SOURCE OF FUNDING NUMBERS

PROGRAM ELEMENT NO.	PROJECT NO.	TASK NO.	WORK UNIT ACCESSION NO.
62101F	6690	669017	669017AB

11. TITLE (Include Security Classification)
Auroral Electron Energy and Flux from Molecular Nitrogen Ultraviolet Emissions Observed by the S3-4 Satellite.

12. PERSONAL AUTHOR(S)
M. Ishimoto and C.I. Meng; G.J. Romick*; R.E. Huffman**

13a. TYPE OF REPORT	13b. TIME COVERED	14. DATE OF REPORT (Year, Month, Day)	15. PAGE COUNT
Reprint	FROM _____ TO _____	1989 August 29	

16. SUPPLEMENTARY NOTATION
Reprinted from J of Geophysical Research, Vol 93, #A9, pp 9854-9866, 1 Sep 1988
* KIA Consultants, Inc; Fairbanks, Alaska
** GL/LIU, Hanscom AFB, MA 01731

17. COSATI CODES		
FIELD	GROUP	SUB-GROUP
0401	170502	

18. SUBJECT TERMS (Continue on reverse if necessary and identify by block number)
AURORA, NITROGEN BANDS
ULTRAVIOLET, SATELLITE

19. ABSTRACT (Continue on reverse if necessary and identify by block number)

The UV spectra over the southern hemisphere nightside auroral oval have been obtained from an AFGL spectral/photometric experiment on board the low-altitude polar-orbiting S3-4 satellite. A detailed analysis of nightside auroral spectra from seven orbits between mid-May and June 1978 was performed to estimate the average energy and total energy flux of incident electrons. This study was based on observations of the N_2 LBH (3-10)(1928 Å) band and the N_2 VK(0-5)(2604 Å) band emission intensities and the application model calculations by Strickland et al. [1983] and Daniell and Strickland [1986]. Comparison of the estimated quantities with the statistical satellite measurement of incident particles by Hardy et al. [1985] indicates that the LBH (3-10) band emission intensity can be used to estimate the total energy flux of incident electrons, s similar to the N_2^+ 1N (0-0)(3914 Å) band emission intensity in the visible region. In addition, the ratio of the LBH (3-10 to the VK(0-5) band emission intensities indicates th average energy of incident auroral electrons in much the same way that the N_2^+ 1N(0-0)

20. DISTRIBUTION/AVAILABILITY OF ABSTRACT	21. ABSTRACT SECURITY CLASSIFICATION
☐ UNCLASSIFIED/UNLIMITED ☒ SAME AS RPT ☐ DTIC USERS	UNCLASSIFIED

22a. NAME OF RESPONSIBLE INDIVIDUAL	22b TELEPHONE (Include Area Code)	22c. OFFICE SYMBOL
ROBERT E. HUFFMAN	(617)377-3311	GL/LIU

DD FORM 1473, 84 MAR 83 APR edition may be used until exhausted. All other editions are obsolete.

SECURITY CLASSIFICATION OF THIS PAGE
UNCLASSIFIED

and OI(6300 Å) emission ratio does in the visible region. This study shows the use of different constituents emissions, model calculations, and synthetic spectra to infer the inherent possibilities in these types of studies.